17èmes JOURNEES DE L'HYDRODYNAMIQUE
JH2020

24 - 26 novembre 2020
CHERBOURG - en - COTENTIN

EFFECT OF LEADING AND TRAILING EDGE FLAPS ON HIGH PERFORMANCE HYDROFOIL TO POSTPONE CAVITATION

17emes JOURNEES DE L'HYDRODYNAMIQUE JH2020

F. Mohammed Arab[(1),*], B. Augier[(2)], F. Deniset[(1)], P. Casari[(3)], and J. A. Astolfi[(1)]

[(1)]Institut de Recherche de l'Ecole Navale IRENav EA 3634, Brest
[(2)]Institut Français de Recherche pour l'Exploitation de la Mer, IFREMER, Brest
[(3)]Institut de Recherche en Génie Civil et Mécanique, GeM, Saint-Nazaire
[*]Corresponding author : fatiha.mohammed_arab@ecole-navale.fr

Summary

For the high-performance foiling yachts, cavitation is often a limiting factor for take-off and top speed. The present work investigates solutions to delay the onset of cavitation thanks to a combination of leading edge and trailing edge flaps. Both numerical studies based on a potential code and experiments in a hydrodynamic tunnel are conducted in order to assess the effect of specific geometric parameters on the hydrodynamic performance and cavitation inception. Experimentally the effect on the hydrodynamic performances and cavitation buckets of a 70% chord trailing edge flap and a 20% chord leading edge flap of NACA 0012 is investigated. The hydrofoils are manufactured using a 3D printer technique at IRENav and tested in the cavitation tunnel of the institute at an inflow velocity of 6.67 m/s ($Re = 10^6$). The results show that the lift coefficient increases and the cavitation bucket gets larger with the flap deflection. The experimental results are in good agreement with the numerical ones by highlighting the capacity of the flaps to enlarge both the operating domain and the cavitation bucket of the hydrofoil.

Résumé

Pour les hydrofoils à hautes performances, la cavitation est souvent un facteur limitant pour le décollage et les hautes vitesses. Ce travail présente des solutions pour retarder l'apparition de la cavitation grâce à une combinaison de volets de bord d'attaque et de bord de fuite. Des études numériques basées sur un code potentiel et des expériences dans un tunnel hydrodynamique sont menées afin d'évaluer l'effet de ces paramètres géométriques sur les performances hydrodynamiques et l'apparition de la cavitation. Les résultats du code potentiel Xfoil de l'hydrofoil avec volets sont évalués par une analyse d'écoulement 2D autour du profil NACA 0012 en utilisant le logiciel Fluent. Expérimentalement, l'effet sur les performances hydrodynamiques et les cartes de cavitation d'un volet de bord de fuite de 70% de la corde et d'un volet de bord d'attaque de 20% de la corde du profil NACA 0012 est étudié. Les hydrofoils sont fabriqués à l'aide d'une technique d'impression 3D à l'IRENav et testés dans le tunnel de cavitation de l'institut à une vitesse d'écoulement de 6.67 m/s ($Re = 10^6$). Les résultats montrent que les volets permettent d'élargir le domaine de fonctionnement en régime sub-cavitant en repoussant l'apparition de la cavitation. Les résultats expérimentaux sont en bon accord avec les résultats numériques.

1. Introduction

If the new hydrofoil technologies used on sailing boats are intended to improve the hydrodynamic forces, cavitation is often a limiting factor for take-off and top speed.

Using this new concept of hydrofoils allow the control of the lift and drag forces for various operating conditions, but this can lead to cavitation onset at high speed and moderate angles of incidence but also at low speed and high angles. Improving the hydrodynamic performances and delaying the cavitation inception requires the modification of shape, hence the idea of using morphing hydrofoils.

The use of morphing structures is particularly analyzed in aerodynamic applications including flying performance [1]. Jawahar et al. [2] analyzed experimentally and numerically the effect of camber flaps on the pressure distribution, on the lift and drag forces as well as the effect on the wake flow. They concluded that the camber of flaps significantly affects the aerodynamic performance and the downstream wake development of the airfoil. The increase of the camberred flap profiles increase the lift coefficients and reduce the lift-to-drag ratio. The aerodynamic performance and mechanical properties of a flexible suction side of an airfoil powered by two actuators are numerically investigated by Brailovski et al. [3].

The gap present at the spanwise ends of the control surfaces is one of the sources of noise and drag. Woods et al. [4] have replaced this gap by a smooth, three-dimensional morphing transition section that elastically lofts between the rigid wing and moving control surface in a passive and continuous manner. The passive control of this compliant morphing flap transition has the advantage of increasing the lift and reducing the drag. The effect of various variable camber continuous trailing edge flap (VCCTEF) on the lift and drag forces is discussed by Kaul et al. [5]. It was noted that the best stall performance (L/D) was demonstrated by the circular and parabolic arc camber flaps.

The most objectives of the hydrodynamic application are similar to those of the aerodynamic applications. So, the airfoil technology can be used in the design of the hydrofoil by taking into account the differences between the fluid properties and the cavitation phenomena. To meet hydrodynamic requirements, adaptive composites are used in many marine technologies including propulsive devices, underwater vehicles, and propellers. In [6], the authors summarized the progress on the numerical modeling, the experimental studies, design and optimization of adaptive composite marine propulsors and turbines.

In order to assess the effect of the cavitation on the structural response, Ducoin et al. [7] have studied the displacement of a flexible homogeneous POM hydrofoil in a cavitating flow. They found that the hydrodynamic loading unsteadiness increases the vibrations experienced by the hydrofoil. Numerically, Garg et al. [8]-[9] have developed a shape optimization tool to predict the hydrodynamic performance including the cavitation inception conditions.

The French Naval Academy Research Institute (IRENav) is interested in the study of the deformed hydrofoils, their responses and enlarging their operating domain. Experimentally, the Fluid-Structure Interaction has been investigated by studying the structural response of a flexible lightweight hydrofoil undergoing various flow conditions including cavitating flow by Lelong et al. [10]- [11]. An optimization of the design and the elastic characteristics of a hydrofoil equipped with deformable elements providing flexibility to the trailing edge was developed by Sacher et al. [12]. In their study, Mohammed Arab et al. [13] analyzed experimentally and numerically the effect of an imposed internal pressure of a compliant composite hydrofoil. It is shown that pressure driven compliant composite structure allows to enlarge the operational domain of the compliant hydrofoil. Also, they found that cavitation can be controlled to some extent by changing only the internal pressure for a given angle of attack and a given inflow velocity.

This paper presents an experimental and numerical study where the effect of the leading and trailing edge deflections of a hydrofoil on its operating domain is investigated. At first, the effect of the leading and trailing edge flaps on the hydrodynamic performance is predicted using Xfoil software. Then, several hydrofoils are manufactured using 3D printing and tested in the cavitation tunnel at IRENav. The paper describes the experimental setup, the numerical computations and presents the main results.

2. Experimental setup

The experiments are carried out in the cavitation tunnel at IRENav (Figure 1). The tunnel test section is 1 m length with a square section of 0.192 m side. The inflow velocity ranges between 0.5 and 15 m/s. The pressure in the tunnel test section ranges between 0.1 bar and 3 bar to control the cavitation which is given by a cavitation number defined by equation 1 and the measured turbulence intensity in the test section is 2% at 5 m/s. This cavitation number can therefore be compared with the opposite of pressure coefficient $-C_{pmin}$ defined as the minimum of the pressure coefficient (equation 2).

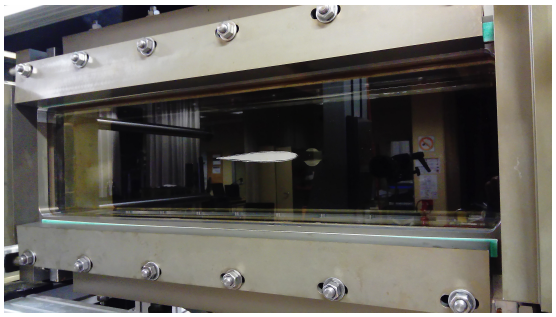

Figure 1. Hydrodynamic tunnel test section at IRENav with the NACA 0012 Profile.

$$\sigma = \frac{P_{ref} - P_v}{\frac{1}{2}\rho V^2} \tag{1}$$

$$C_p = \frac{P - P_{ref}}{\frac{1}{2}\rho V^2} \tag{2}$$

Where P_{ref} is the pressure in the test section, P_v is the vapor pressure at the water temperature, P is the local pressure, V is the inflow velocity, and ρ is the water density. Thus, when $\sigma < -C_{pmin}$, that is to say when $P < P_v$, cavitation is expected to appear in the flow at the point where the pressure coefficient is the lowest.

Four hydrofoils of plastic (PLA) are manufactured using an additive process or 3D printing techniques and tested in the hydrodynamic tunnel at IRENav.These hydrofoils have 0.15 m chord length and 0.191 m span. The first one is a symmetrical NACA 0012 and the other have a difference at the type, the flap deflection angles and the rotating position. The different angles involved are described in figure 2. α is the angle of incidence, γ is the angle of the leading edge flap and β is the angle of the trailing edge flap.

Figure 2. Schematic diagram of the different angles: angle of incidence (α), angle of the leading edge flap (γ) and angle of the trailing edge flap (β).

Figure 3 shows the four hydrofoil geometries used in this study. One of the hydrofoils has a leading edge flap at 20%c with the deflection angle of $\gamma = 3°$, the second one has a trailing edge flap at 70%c with the deflection angle of $\beta = 5°$ and the last one has the two flaps: leading edge flap at 20%c with the deflection angle of $\gamma = 3°$ and trailing edge flap at 70%c with the deflection angle of $\beta = 5°$. These hydrofoils have 0.15 m chord length and 0.191 m span.

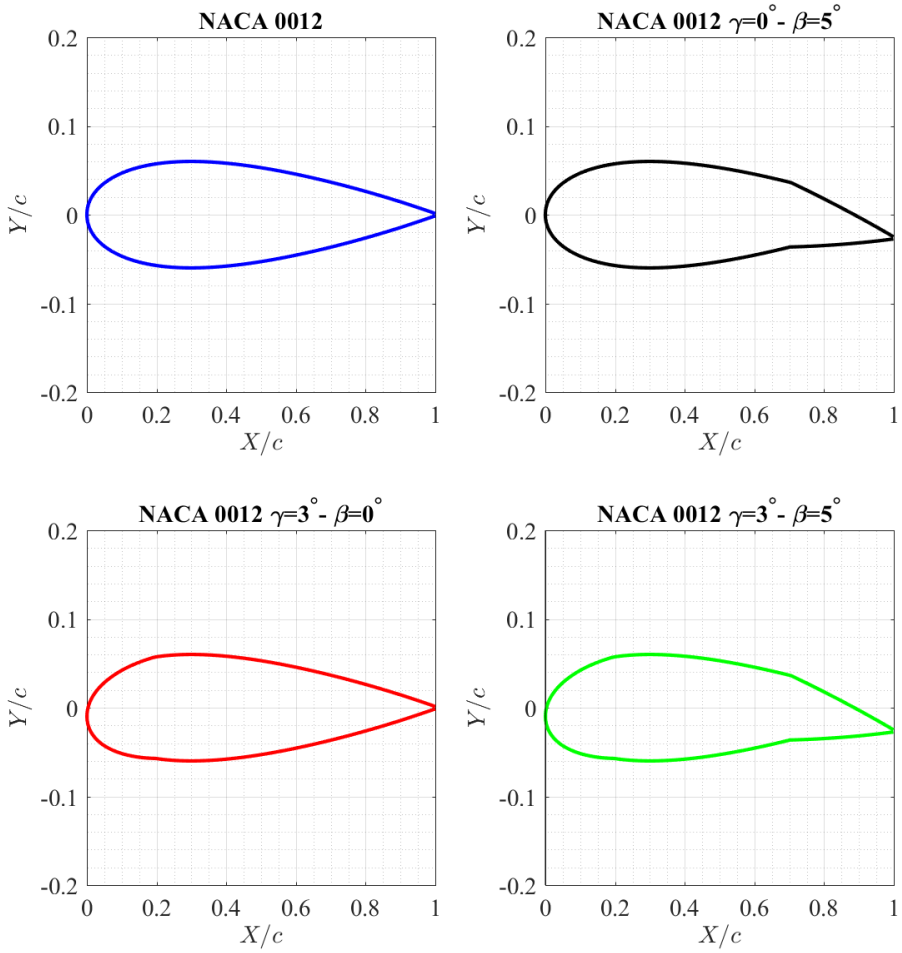

Figure 3. NACA 0012 profile and hydrofoils shapes with different flaps.

The hydrofoils are mounted in the test section using a new system developed in the institute which is named fairing system. To measure the components of the hydrodynamic forces, the hydrofoils are mounted on an axis of rotation at $X/c = 0.25$. The axis of rotation is made of stainless steel to avoid the bending of the hydrofoil. The axis of rotation has a rectangular form and is fastened into the hydrodynamic balance, secured by a tight fitted key/nut system. Then, the hydrofoils are mounted by the front wall of the test section in order not to disturb the setting of the hydrodynamic balance. The figure 4a presents the schematic of the NACA 0012 hydrofoil and the fairing system.

Example of 3D printing hydrofoil and CAD of the NACA 0012 with traditional mounting system are presented in figure 4b.

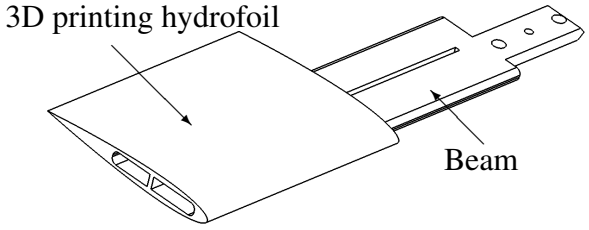

(a). CAD of NACA 0012 with hydrofoil fairing system

(b). 3D printing NACA 0012 with fairing system

Figure 4. Schematic and image of a 3D printing NACA 0012.

At first, preliminary tests are carried out in order to validate the efficiency of the new mounting system (fairing system). The hydrodynamic coefficients measured on the cantilevered NACA 66312 made of stainless steel are compared to the measurements obtained on the 3D printing NACA 66312 mounted using a fairing system. Figure 5 presents the NACA 66312, which has 0.1 m chord and 0.191 m span. The experiments are carried out in the cavitation tunnel at Reynolds number of $Re = 5.33\ 10^5$ and angle of attack ranges between -10° and $+10^\circ$.

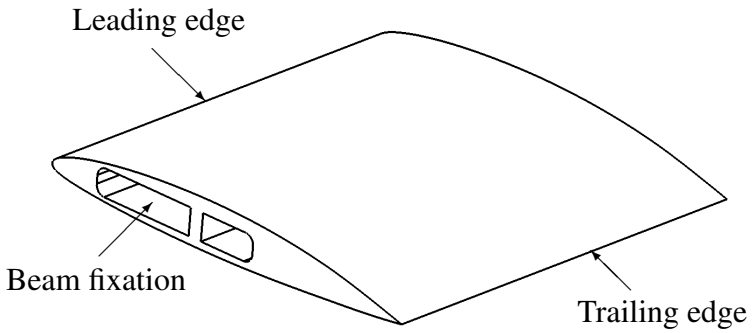

Figure 5. CAD of NACA 66312 with hydrofoil fairing system.

In the hydrodynamic tunnel, measurement of hydrodynamic forces is performed using a hydrodynamic balance at various conditions of angle of attack at an inflow velocity of 6.67 m/s corresponding to a Reynolds number of 10^6. The 5-component hydrodynamic balance has a range up to 1700 N for the lift force, 180 N for the drag and a 43 Nm for the pitching moment. It is fixed into a supporting frame, mounted on bearings, and driven in rotation by a Baldor motor. The stepper motor allows for 600 000 impulsions per rotation, meaning a resolution of $6\ 10^{-4\circ}$. The foil is fastened into the balance, secured by a tight fitted key/nut system [14]. As the test section is horizontal, the geometric 0° angle of attack of the hydrofoil is visually controlled using the water surface at mid height of the test section when filling the tunnel. Also, as the first hydrofoil is symmetric, the zero-lift angle is used for the final angle of attack positioning.

To plot experimentally the cavitation bucket for various cavitation numbers, the inflow velocity is fixed at 6.67 m/s. The cavitation was visually observed under stroboscopic light. The inception condition was determined by increasing the angle of attack at a constant cavitation number until cavitation appeared. It consist in determining the angles and the lift coefficients for which cavitation occurred on both suction and pressure sides for a constant cavitation number. The cavitation inception is considered when an organized spanwise cavitation pattern was visually detectable along a significant portion of the leading edge. For the low cavitation numbers, the inception angle was determined until the first bubbles were visually detected on the suction side.

3. Uncertainties

In the cavitation tunnel, the uncertainties of velocity and pressure measurements are based on the accuracy of the pressure sensors. The latter is about 0.04 bar. For the measurements of hydrodynamic forces and from the document provided by the manufacturer of the hydrodynamic balance, the uncertainties are about ± 1.02 N for the lift, ± 0.324 $N$for the drag and ± 0.26 $N.m$ for the pitching moment.

4. Numerical approach

The numerical study consists of 2D simulation to investigate the effect of leading and trailing edge deflections on the hydrodynamic performances.

The hydrofoils shapes are plotted using a direct foil design menu of Xfoil, which allows us to define the leading and trailing edge deflections and the rotating flaps position. After, the flow model of the Xfoil solver is used to evaluate the hydrodynamic performances. The flow model is based on the coupling a panel method

and a boundary layer model. More details on Xfoil are given in [15]. The panel method accelerates the flow calculations as compared to finite volume methods.

The simulations are carried out for a velocity of 6.67 m/s corresponding to a Reynolds number of 10^6 and different angles of attack.

5. Results and discussion

5.1 Numerical results

The effect of the leading and trailing edge deflection angles is predicted using Xfoil software. Figure 6 illustrates the numerical lift coefficients of the different hydrofoils. It is very clear that the trailing edge flap increases the lift coefficient of the hydrofoil. At the opposite, the leading edge deflection angle has no effect on the lift coefficient. For the same angle of attack ($\alpha = 2°$), the trailing edge flap increases the lift coefficient about 0.35. When, the same operating point $C_L = 0.5$ is considered, the trailing edge $\beta = 5°$ decreases the angle of attack from 4.48° to 1.35° ($\Delta\alpha = 3.13°$).

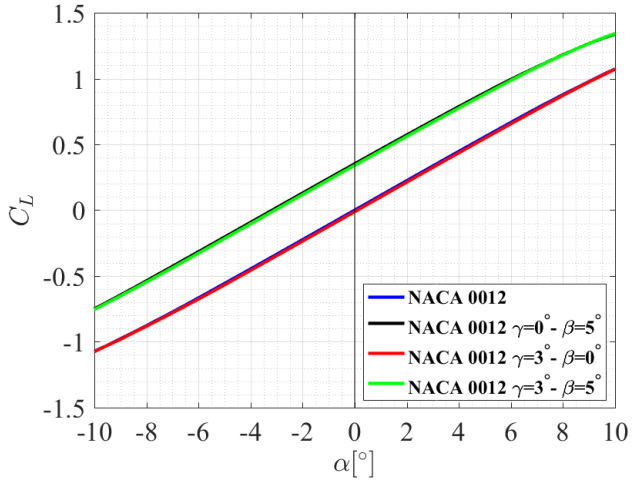

Figure 6. Numerical effect of the leading edge and trailing edge flaps on the lift coefficient evolution as a function of the angle of attack, $Re = 10^6$.

The effect of the flaps deflections on the cavitation inception is also predicted using Xfoil analysis. Figure 7 shows the lift coefficient versus the opposite of the minimum pressure coefficient ($-C_{pmin}$) of the symmetrical hydrofoil and profiles with leading edge flap of $\gamma = 3°$ at 20%c, trailing edge flap of $\beta = 5°$ at 70%c and profile with leading and trailing edge deflections $\gamma = 3°$ and $\beta = 5°$.

The flaps deflection has a direct influence on the theoretical cavitation inception, particularly for lift coefficients larger than 0.075. It is found that the leading and trailing edges deflections enlarge the non-cavitation domain. For the low lift coefficients, the trailing edge flap is sufficient to delay the cavitation inception. For the high lift coefficients, the leading edge flap is necessary to enlarge the non-cavitation domain and it gives a significant gain.

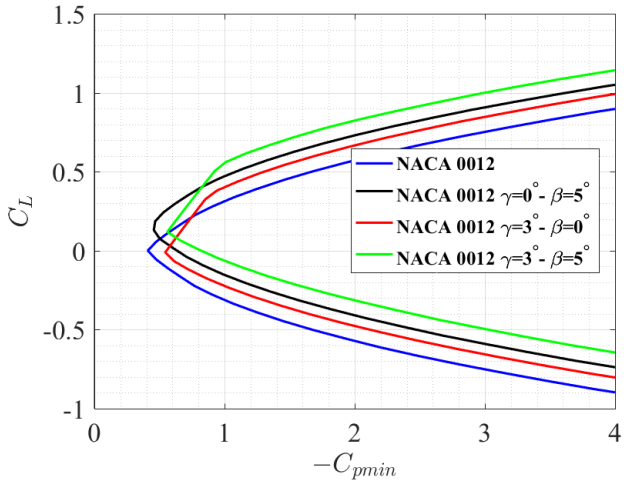

Figure 7. Numerical cavitation bucket of NACA 0012, NACA 0012 with leading edge flap, NACA 0012 with trailing edge flap and NACA 0012 with leading and trailing edge flaps, $Re = 10^6$.

5.2 Validation of the fairing system

The hydrodynamic coefficients measured on the PLA hydrofoils mounted using a fairing system are compared to those measured on the stainless steel hydrofoil mounted using the traditional mounting system. These experimental results are also compared to the numerical ones calculated with the 2D section of the NACA 66312 profile using Xfoil. The computations were carried out for a Reynolds number of $Re = 5.33\ 10^5$, $N_{crit} = 9$ and the transition was forced to 5% of the chord.

The experimental evolution of the lift and drag coefficients as a function of the angle of attack are presented respectively in figure 8a and figure 8b. They summarized the experimental coefficients measured on the hydrofoil made of stainless steel and on the hydrofoils printed using 3D printer technique. These results are compared to the numerical ones predicted by Xfoil.

It is shown that the lift coefficient measured on the stainless steel profile has the same trend as the one measured on hydrofoils manufactured in 3D printing. The same remark is obtained for the drag coefficient. During this analysis, the maximum difference between the experimental lift coefficients is about 0.087. This difference was noted at $\alpha = -10°$ angle of incidence between the stainless steel profile and the first PLA profile. For the drag coefficient, the maximum difference is obtained for the same angle of incidence ($\alpha = -10°$) and it was over 0.0304. Far from the stall area, the maximum difference between the C_L measured on the hydrofoils made of the stainless steel and the PLA1 is about of 0.076 noted at $\alpha = 6°$.

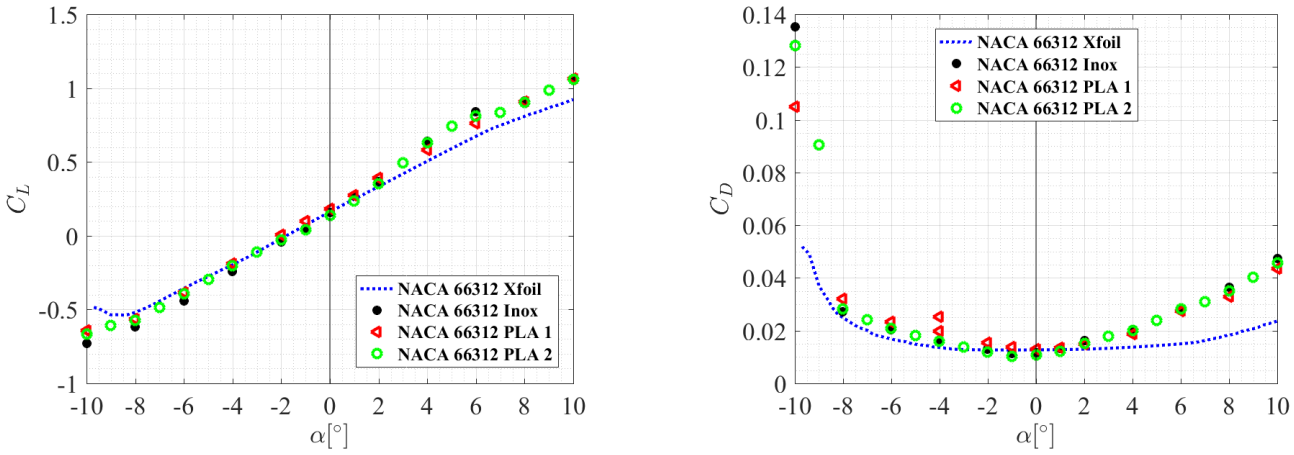

(a). Lift coefficient (b). Drag coefficient

Figure 8. Experimental and numerical lift and drag coefficients of the NACA 66312 hydrofoils made of stainless steel and PLA, $Re = 5.33\ 10^5$.

The comparison of the experimental results to the numerical ones given by Xfoil shows that the lift coefficient measured on the different hydrofoils fits well with that predicted by the computations. A difference of 0.15 was obtained between the numerical results and the experimental ones measured on hydrofoil made of PLA at 5° angle of incidence. On the other hand, the analysis of the evolution of the drag coefficient shows that the Xfoil software underestimates the drag of the NACA 66312. This difference is due to the 3D effect of the drag in the cavitation tunnel.

The cavitation inception on the NACA 66312 hydrofoils made using 3D printer technique is compared to the cavitation inception obtained on the same type of hydrofoil made of stainless steel. The latter is cantilevered and clamped on a cylindrical aluminium beam fitted to the hydrodynamic balance and the hydrofoils made using 3D printer technique are mounted using a fairing system. The various measurement campaigns were carried out at $5.33\ 10^5$ Reynolds number. The results of these tests are compared to those predicted by the Xfoil software under the same flow conditions. The experimental and the numerical cavitation buckets are presented in figure 9.

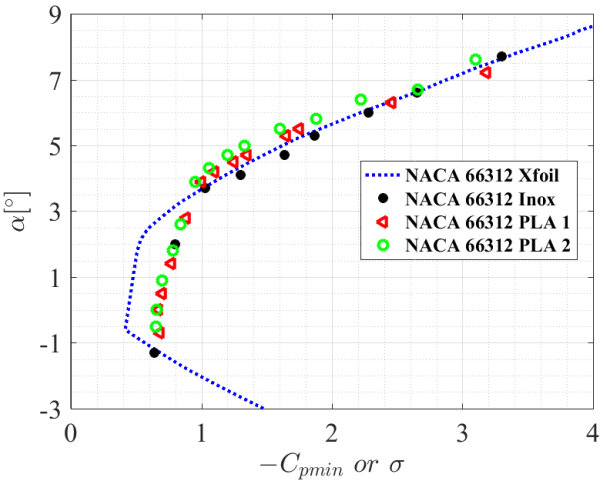

Figure 9. Experimental and numerical cavitation buckets of NACA 66312 made of stainless steel and of PLA, $Re = 5.33\ 10^5$.

The conditions of cavitation inception on the PLA hydrofoils suction side are similar to those of cavitation inception on the stainless steel hydrofoil. However, the values are lower for the stainless steel hydrofoil. The order of maximum difference between the angles of the cavitation inception on the stainless steel hydrofoil

and the hydrofoil made of PLA is about $\Delta\alpha = 0.8°$ noted at the cavitation numbers $\sigma = 1.6$ and $\sigma = 1.3$. This difference can be explained by the criterion of the cavitation inception and the step of incidence $\Delta\alpha$ chosen, thus the fluctuations of speed and pressure in the test section.

5.3 Experimental results of the effect of flap on the hydrodynamic performance

The hydrofoils manufactured using the 3D printer technique are studied in cavitation tunnel at IRENav. For a Reynolds number of 10^6, the lift coefficients measured using the hydrodynamic balance are presented in figure 10a. These experimental results are compared to the numerical ones obtained from the numerical study. The experimental results for the four hydrofoils fit very well with the numerical ones (figure 10b).

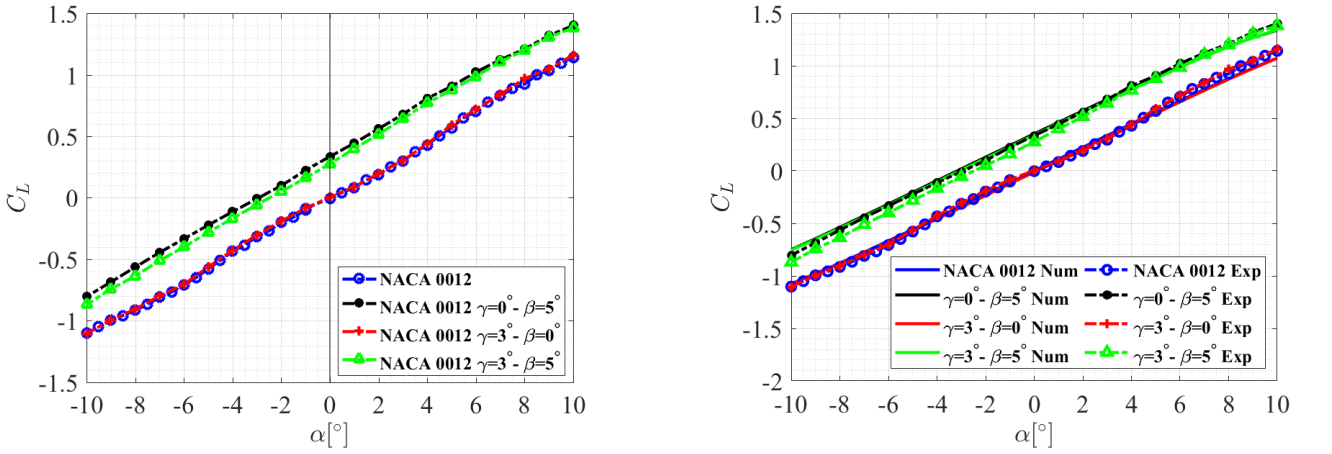

(a). Experimental lift coefficients (b). Experimental and numerical lift coefficients

Figure 10. Experimental and numerical lift coefficients of the hydrofoils, $Re = 10^6$.

The experimental and numerical lift-to-drag ratios are plotted in figure 11. It is shown that the trailing edge deflection improves the lift-to-drag ratio for an angle of attack below the stall angle. The experimental and numerical lift-to-drag ratios have the same trend evolution but a significant difference in terms of magnitude. So, Xfoil tends to under-predict drag coefficients and slightly over-predict lift-to-drag ratios.

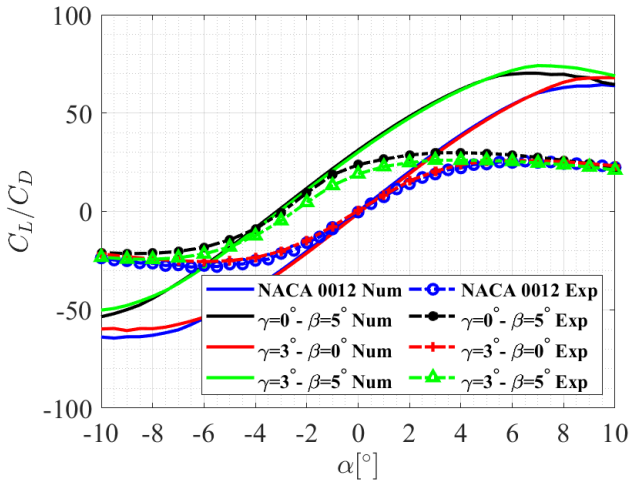

Figure 11. Experimental lift/drag ratio (C_L/C_D) as a function of the angle of attack of the hydrofoils, $Re = 10^6$.

For each hydrofoil and various cavitation numbers, the cavitation inception and desinence are investigated in the test section of the cavitation tunnel at IRENav. The cavitation inception and desinence are compared

to the theoretical bucket predicted using Xfoil as presented in figure 12 which summarizes the conditions for cavitation inception and desinence on the hydrofoil surface. The abscissa denotes the cavitation number and the ordinate denotes the lift coefficient for which cavitation was visually detectable. A good agreement is found between the numerical and the experimental results, particularly the cavitation desinence and for the low lift coefficients. For $C_L > 0.6$ the experimental cavitation bucket discard from the numerical ones. An hysteresis between the cavitation inception and desinence for the same cavitation number is observed. This hysteresis means that the pressure required for the cavitation inception must be less than the pressure required for the cavitation desinence.

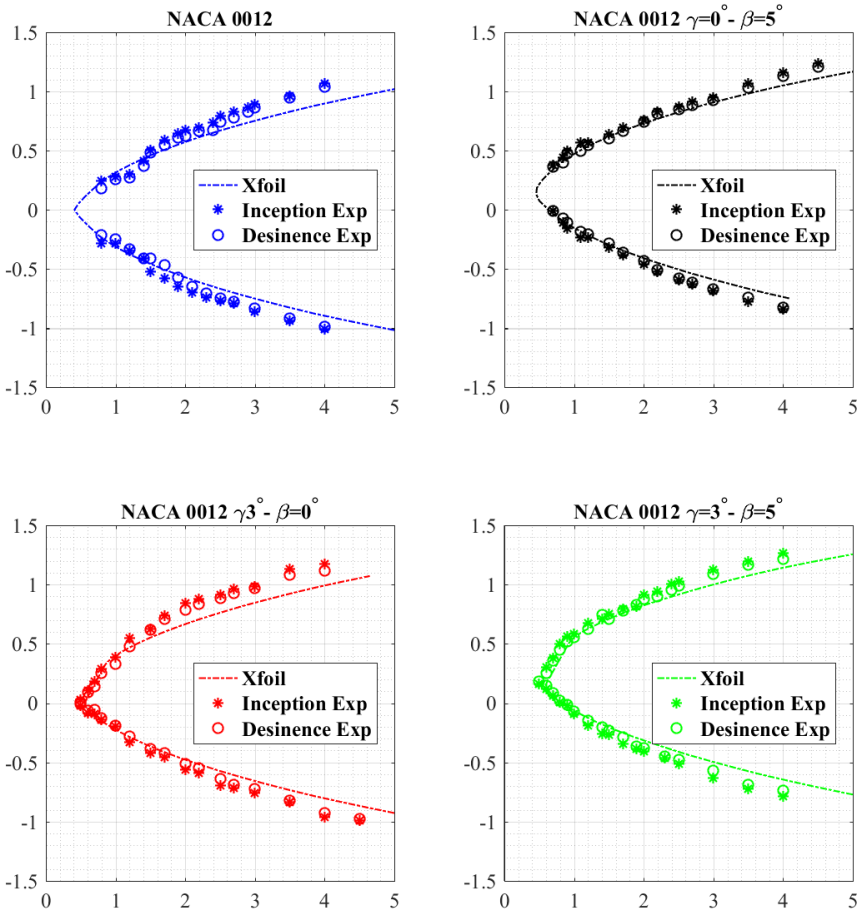

Figure 12. Experimental cavitation inception and desinence compared to the numerical ones of the NACA 0012 and hydrofoils with flaps, $Re = 10^6$.

In the aim to highlight the advantage of the leading and trailing edge flaps, the variation of cavitation number for the same operating point is extracted. For the same lift coefficient $C_L = 0.5$, the non cavitation domain enlarges about $\Delta\sigma = 0.7$. In the case of the immersion of the hydrofoil of $h = 1\ m$, this variation corresponds to a speed of 4.42 m/s.

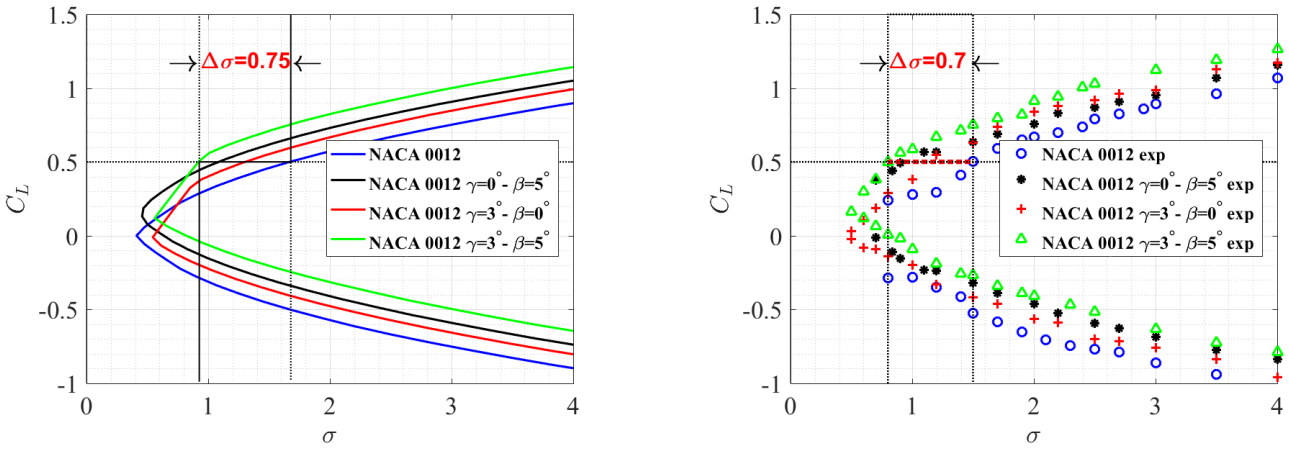

(a). Numerical results (b). Experimental results

Figure 13. Effect of the flaps on the experimental and numerical cavitation buckets of the NACA 0012, $Re = 10^6$.

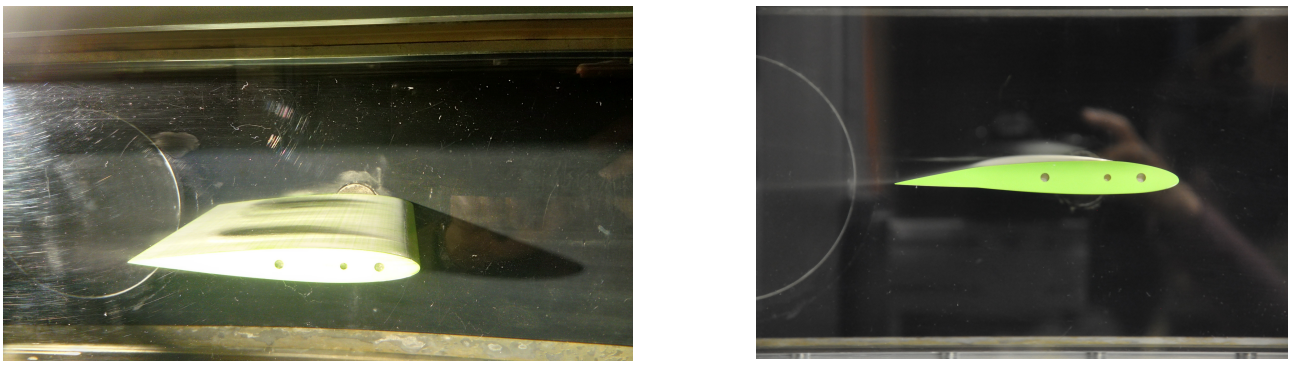

(a). NACA 0012 (b). NACA 0012 with flaps $\gamma = 3°$ et $\beta = 5°$

Figure 14. Experimental cavitation inception on the hydrofoil surfaces, $Re = 10^6$.

6. Conclusions

In this paper, an experimental and numerical study has been presented in order to assess the effect of the leading and trailing edge flaps on the hydrodynamic performance of a symmetrical hydrofoil.

Numerically, the effect of the leading and trailing edge flaps deflection angles on the hydrodynamic coefficients and cavitation bucket is predicted at $Re = 10^6$ using Xfoil software.

Experimentally, four hydrofoils are manufactured using 3D printer technique and tested in the hydrodynamic tunnel at IRENav. The first hydrofoil is a reference one NACA 0012 without flaps, the second hydrofoil has a trailing edge flap of $\beta = 5°$ at 70%c, the third one has a leading edge flap of $\gamma = 3°$ at 20%c and the last hydrofoil has a leading and trailing edge flaps of $\gamma = 3°$ and $\beta = 5°$. The hydrodynamic forces are measured using the hydrodynamic balance at a Reynolds number of $Re = 10^6$ and different angles of attack. To analyze the cavitation inception, the experimental cavitation buckets are plotted for the different hydrofoils and compared to the theoretical ones calculated by Xfoil.

The Xfoil simulations show that the trailing edge deflection angle increases the lift coefficient, contrary to the leading edge that has no effect on the hydrodynamic forces. It is also noted that the leading and trailing edge deflections enlarge the non-cavitation domain of a symmetrical hydrofoil (NACA 0012). The results of these simulations are compared to the experimental ones obtained from the tests in the cavitation tunnel at IRENav. It is concluded that the numerical results are in good agreement with experimental ones.

Acknowledgments

The authors would like to thank the technical staff of the French Naval Academy Research Institute for their support to this study.

Nomenclature

α	angle of attack [°].
β	trailing edge deflection [°].
γ	leading edge deflection [°].
ρ	fluid density [kg/m^3].
σ	cavitation number: $\sigma = \frac{P-P_v}{\frac{1}{2}\rho V^2}$ [-].
c	hydrofoil chord [m].
C_D	drag coefficient: $C_D = \frac{D}{\frac{1}{2}\rho V^2 s}$ [-].
C_L	lift coefficient: $C_L = \frac{L}{\frac{1}{2}\rho V^2 s}$ [-].
D	drag force [N].
e	hydrofoil span [m].
L	lift force [N].
P	pressure [bar].
Re	Reynolds number: $Re = Vc/\nu$ [-].
s	hydrofoil planform [m^2].
V	inflow velocity [m/s].
X, Y, Z	foil coordinates [m].
ν	kinematic viscosity [m^2/s].

References

[1] I. Dimino, L. Lecce, and R. Pecora, *Morphing Wing Technologies: Large Commercial Aircraft and Civil Helicopters*. Butterworth-Heinemann, 2017.

[2] H. K. Jawahar, Q. Ai, and M. Azarpeyvand, "Experimental and numerical investigation of aerodynamic performance for airfoils with morphed trailing edges," *Renewable energy*, vol. 127, pp. 355–367, 2018.

[3] V. Brailovski, P. Terriault, D. Coutu, T. Georges, E. Morellon, C. Fischer, and S. Bérubé, "Morphing laminar wing with flexible extrados powered by shape memory alloy actuators," *In ASME 2008 Conference on Smart Materials, Adaptive Structures and Intelligent Systems. American Society of Mechanical Engineers*, pp. 615–623, 2008.

[4] B. K. Woods, L. Parsons, A. B. Coles, J. H. Fincham, and M. I. Friswell, "Morphing elastically lofted transition for active camber control surfaces," *Aerospace Science and Technology*, vol. 55, pp. 439–448, 2016.

[5] U. K. Kaul and N. T. Nguyen, "Drag characterization study of variable camber continuous trailing edge flap," *Journal of Fluids Engineering*, vol. 140, no. 10, p. 101108, 2018.

[6] Y. L. Young, M. R. Motley, R. Barber, E. J. Chae, and N. Garg, "Adaptive composite marine propulsors and turbines: progress and challenges," *Applied Mechanics Reviews*, vol. 68, no. 6, p. 060803, 2016.

[7] A. Ducoin, J. A. Astolfi, and J. F. Sigrist, "An experimental analysis of fluid structure interaction on a flexible hydrofoil in various flow regimes including cavitating flow," *European Journal of Mechanics-B/Fluids*, pp. 63–74, 2012.

[8] N. Garg, Z. Lyu, T. Dhert, J. Martins, and Y. L. Young, "High-fidelity hydrodynamic shape optimization of a 3-d morphing hydrofoil," *Fourth International Symposium on Marine Propulsors*, 2015.

[9] N. Garg, G. K. Kenway, J. R. Martins, and Y. L. Young, "High-fidelity multipoint hydrostructural optimization of a 3-d hydrofoil," *Journal of Fluids and Structures*, vol. 71, pp. 15–39, 2017.

[10] A. Lelong, P. Guiffant, and J. A. Astolfi, "An experimental analysis of the structural response of flexible lightweight hydrofoils in cavitating flow," *Journal of Fluids Engineering*, vol. 140, no. 2, p. 021116, 2018.

[11] A. Lelong, P. Guiffant, and J. A. Astolfi, "An experimental analysis of the structural response of flexible lightweight hydrofoils in various flow conditions," *16th International Symposium on Transport Phenomena and Dynamics of Rotating Machinery*, 2016.

[12] M. Sacher, M. Durand, E. Berrini, F. Hauville, R. Duvigneau, O. Le Maitre, and J. A. Astolfi, "Flexible hydrofoil optimization for the 35th america's cup with constrained ego method," *Ocean Engineering*, vol. 157, pp. 62–72, 2018.

[13] F. M. Arab, B. Augier, F. Deniset, P. Casari, and J. A. Astolfi, "Morphing hydrofoil model driven by compliant composite structure and internal pressure," *Journal of Marine Science and Engineering*, vol. 7, no. 12, p. 423, 2019.

[14] J. B. Marchand, J. A. Astolfi, and P. Bot, "Discontinuity of lift on a hydrofoil in reversed flow for tidal turbine application," *European Journal of Mechanics-B/Fluids*, vol. 63, pp. 90–99, 2017.

[15] M. Drela, "Xfoil: An analysis and design system for low reynolds number airfoils," in *Low Reynolds number aerodynamics*, pp. 1–12, Springer, 1989.